A small cavity for detecting sound-induced flow

Junpeng Lai,[1,a)] Zihan Liu,[1] Morteza Karimi,[1] Mahdi Farahikia,[2] Weili Cui,[3] Johar Pourghader,[1]
Sara Aghazadeh,[1] Changhong Ke,[1] and Ronald Miles[1,b)]

[1]*Department of Mechanical Engineering, Binghamton University, Binghamton, New York 13902, USA*

[2]*Division of Engineering Programs, State University of New York at New Paltz, New Paltz, New York 12561, USA*

[3]*Department of Mechanical & Facility Engineering, State University of New York, Maritime College, Bronx, New York 10465, USA*

ABSTRACT:

A study is presented of a method for creating an acoustic flow sensor that is generally compatible with current silicon microfabrication processes. An aim of this effort is to obtain a design consisting of a minimal departure from the existing designs employed in mass-produced silicon microphones. Because the primary component in all of these microphones is the cavity behind the pressure-sensing diaphragm, we begin with a study of the acoustic particle velocity within a cavity in a planar surface. The sound within the cavity is caused by the external plane sound wave traveling parallel to the cavity's open surface. It is shown that with suitable dimensions of the cavity, the acoustic particle velocity simultaneously flows inward at one end and outward at the other end of the single open cavity surface. A simple analytical model is presented to estimate the required length and depth of the cavity such that the acoustic particle velocity into and out of the opening is a reasonable approximation to that of a plane traveling sound wave in the free field. Measurements of the acoustic particle velocity into and out of the cavity are in close agreement with both the simple model and a more detailed finite element model. Agreement between two dissimilar modeling approaches and experiments suggests that the dominant features of the system have been accounted for. By redirecting the acoustic particle velocity into and out of the cavity opening rather than the flow being parallel to the plane surface, this configuration greatly facilitates the design and fabrication of structures intended to sense the acoustic flow. © *2025 Acoustical Society of America*. https://doi.org/10.1121/10.0034788

(Received 7 June 2024; revised 25 November 2024; accepted 5 December 2024; published online 7 January 2025)

[Editor: Robert D. White]

Pages: 29–42

I. INTRODUCTION

A pressure-sensing microphone could be viewed as a cavity in a surface along with some means of detecting the sound-induced pressure gradient at the cavity opening. This detection is typically accomplished using a membrane or diaphragm and transducing its motion into an electronic signal. In silicon microphones, the cavity behind the pressure-sensing diaphragm is created by using a through-wafer etch from the backside of the wafer. For examples, see Shah *et al.* (2019) or any introductory acoustics textbook (Miles, 2020). The present study consists of an examination of how this cavity could be designed to facilitate the creation of a silicon microphone that senses flow rather than pressure.

While the goal of this effort is to facilitate microphone design, it is not intended to present a complete candidate flow-microphone design. Our focus is on the starting point rather than on tackling the entire system. The cavity that comprises the essential component of pressure-sensing microphones is one of countless systems that are important in engineering acoustics that involve the interaction of an incident sound wave with a closed volume of air having an opening to the external sound field (Mahesh *et al.*, 2024).

The closed volume is formed using essentially rigid walls with an opening that permits an external sound pressure to produce acoustic fluctuations within the volume. When the dimensions of the opening and the enclosed volume are sufficiently small relative to the sound wavelength, the sound pressure tends to be rather uniform across the opening area and within the volume. This is the configuration of the familiar Helmholtz resonator (Strutt, 1916). Our interest here is with the interaction of an external sound wave with an enclosed volume having a markedly different shape than that of the typical Helmholtz resonator. In an attempt to keep things as simple as possible, the volume will be taken to be rectangular, having a length, width, and depth. The opening to the external field can then be considered to be rectangular with dimensions equal to the length and width of the air volume.

The dimensions of the cavity will be selected such that a sound wave traveling parallel to the surface elicits flow simultaneously into and out of the cavity as depicted in Fig. 1.

Our current interest is to examine the use of this system to facilitate the design of acoustic sensors. As with typical microphones, we will assume that some sort of sensing structure is placed at the opening of the air-filled volume. Because the enclosed air-space differs significantly from the image of a bottle having a narrow neck of the Helmholtz resonator, in the following we will refer to it as a "cavity."

a)Email: jlai16@binghamton.edu
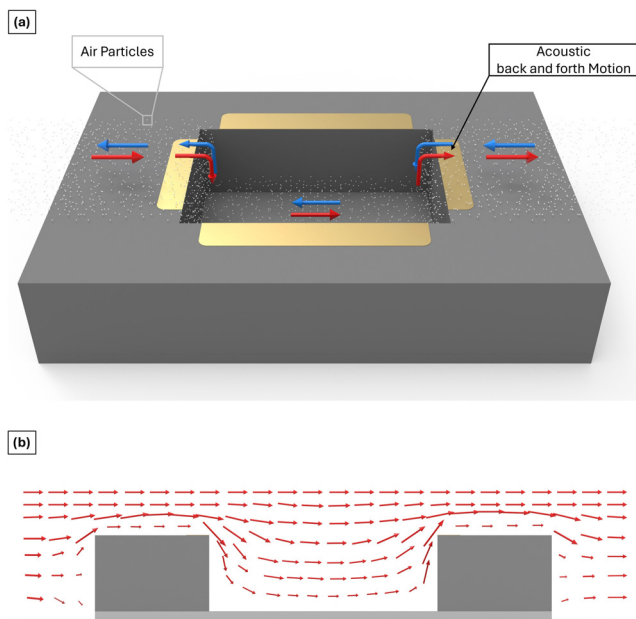b)Email: miles@binghamton.edu

FIG. 1. (Color online) Illustration of the microscale flow-sensing concept. Rather than use structures that are oriented orthogonal to the chip substrate as depicted in Fig. 2, in this study we consider the redirection of the sound-induced flow into and out of a cavity in the chip. The upper panel (a) depicts a perspective view of the chip with flow into and out of the cavity. The direction of the fluctuating flow (into and out) is depicted by the red and blue arrows. When the external fluctuating field consists of acoustic particle flow from left to right, the red arrows depict flow into the cavity on the left side while flow leaves the cavity on the right side. The blue arrows indicate the flow directions when the external field flows from right to left. The lower panel (b) shows a side view with red arrows indicating the direction and magnitude of the flow.

This cavity will be viewed as residing in an infinite (i.e., large relative to the wavelength) plane surface. A plane sound wave travels along the surface in the direction parallel to the length of the cavity.

In referring to the air-filled space behind the acoustic sensing structure as a "cavity," our interest here is on the acoustic behavior of this cavity as used in common acoustic sensors. Of course, typical pressure sensing microphones rely on a diaphragm placed over a back volume of air, i.e., a cavity (Miles, 2020). It is hoped that this will not be confused with other acoustic cavities such as bomb bays in flying vehicles, which are also referred to as cavities. Strong acoustic resonances can occur in bomb bays but these cavities are typically much larger than those of interest here and are subject to notably different flow phenomena including a significant steady free-stream velocity (Bartel and McAvoy, 1981). The essential physical principles involved in the system considered here have little in common with those of such high speed flows. All flow velocities considered here are assumed to fluctuate with the sound frequency and have zero mean when averaged over a period of the oscillation. The Reynold's numbers of the flows considered here are assumed to be extremely small while those of higher speed flows are generally very high.

One could consider countless acoustical effects that could influence the sound field within the air volume. In the

present attempt to create a model of this system, we would like to retain only the most dominant effects in order to elucidate how the primary design parameters influence the sound field. As with the Helmholtz resonator, the small dimensions of this cavity also permit significant simplifications in analyzing the resulting sound field. We will assume that the depth of the enclosed volume is significantly smaller than the sound wavelength so that there is minimal pressure variation through the depth. Unlike the assumptions of the Helmholtz resonator in which it is normally assumed that the incident sound pressure is essentially uniform across the opening, the external sound field will be assumed to consist of a plane traveling wave propagating parallel to the open length of the cavity. The cavity length will be assumed to be small but not negligible relative to the sound wavelength. This assumption permits length-wise variations in the pressure and particle velocity across the opening and within the volume. Because the external sound pressure and particle velocity are uniform in the direction of the cavity width, we will assume the field within the cavity does not vary across the width.

We should also mention that despite the fact that the cavity examined here shares the assumption of small dimensions relative to the sound wavelength with the Helmholtz resonator, we do not consider the present system to be a "resonator," although any acoustic system can resonate. While resonance is a defining feature of the Helmholtz resonator, it is not an essential feature of the system considered here.

The essential acoustical phenomenon in this system is that when the sound wave arrives at the cavity, the acoustic particle velocity experiences an abrupt change of direction; rather than being in the direction of propagation as it is in any plane sound wave, and as occurs along the planar surface before encountering the cavity, it is redirected at the cavity leading edge toward the cavity bottom. Because the cavity dimensions are small relative to the sound wavelength, the air within the cavity can be considered rather incompressible. Consequently, downward flow at the leading edge is accompanied by flow up and out of the cavity at the trailing edge. Again, this is depicted approximately in Fig. 1.

This combination of inward and outward acoustic flow by the cavity can provide a foundation for practical acoustic sensors that detect acoustic particle velocity. Another consequence of the relatively small dimensions of the cavity is that small details of the cavity shape tend to not have a dominant influence on the sound field; small departures from the ideal rectangular shape are not likely to have much influence. A primary aim of the present study is then to determine the approximate cavity dimensions that enable this simultaneous inward and outward air motion.

The required cavity dimensions will be estimated by first constructing a highly simplified mathematical model of the system. Again, while there are countless acoustical effects that could influence the field, our aim is to account only for those that dominate so we obtain the simplest

possible design guidelines. This simple model is then verified experimentally and is found to agree with results obtained using a more detailed finite element model. Having determined the essential dimensions of the cavity to produce this simultaneous inward and outward acoustic flow in the cavity, we then examine how this system could be utilized to facilitate the design of acoustic sensors. Because the geometry of this system produces a redirection of the acoustic particle velocity, we will explore how to employ it in the creation of sensors to detect acoustic particle velocity.

The results given in the following show that the velocity of the acoustic flow into and out of the cavity can be a close approximation to the acoustic flow velocity in the incident plane sound wave propagating parallel to the planar surface in which the cavity resides. Detecting this flow velocity into and out of the cavity could then provide a practical way to measure the acoustic particle velocity in the external field. This could result in a dramatic departure from our usual way of designing acoustic sensors.

Since a key feature of this system is simultaneous flow into and out of the cavity, its use in the creation of a practical acoustic sensor requires some means of detecting the flow. Sound, as detected by humans and most vertebrates, consists of minute fluctuations in pressure which result in displacement of our pressure-sensing tympana. When contemplating designs of microphones, it can be instructive to examine hearing organs in animals, since Nature has a well-deserved reputation for getting things right. Countless animals detect sound without tympana, using fine hairs which are often driven by viscous forces in the air as it moves due to spatial gradients in the fluctuating sound pressure. While the design of microphones has nearly always been inspired by pressure-sensing ears such as our own, it might be that the detection of acoustic flow, or particle velocity, as used by the vast majority of hearing animals e.g., arthropods such as crickets and spiders, many aquatic animals, etc. (Bathellier *et al.*, 2012; Göpfert and Robert, 2000; Tao and Yu, 2012), might prove beneficial in many applications. The use of a cavity to redirect the flow as described in the following could provide a key step in achieving a practical design.

Fine hair-like structures to be used in sensing flow can be fabricated using various methods, including silicon microfabrication, and there have been several designs described in the literature (Dagamseh *et al.*, 2010; Droogendijk *et al.*, 2014; Tao and Yu, 2012). In many cases, these structures are inspired by insect flow-sensing hairs and consist of a relatively rigid structure supported on a flexible hinge that incorporates some sort of sensing mechanism. This structure is often oriented orthogonal to the plane of a silicon chip in order to take advantage of the acoustic flow that is parallel to the chip surface as depicted in Fig. 2. While these structures have been successfully fabricated by researchers and their performance has been demonstrated, the process required to fabricate them presents a dramatic departure from that employed in microphones as fabricated in micro-electro-mechanical systems (MEMS). This greatly discourages their adoption in commercial products.
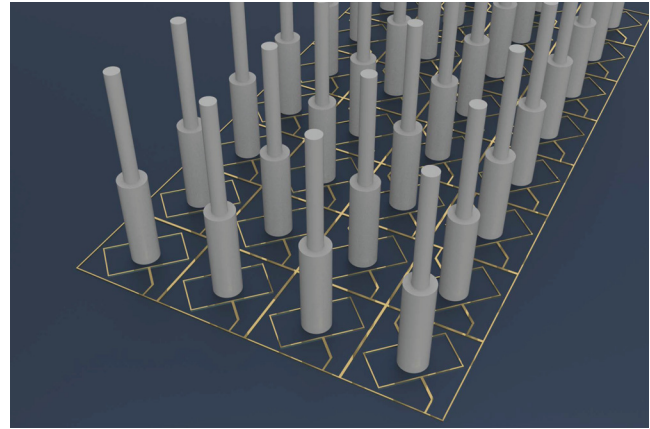

FIG. 2. (Color online) Schematic of a sensor inspired by the flow-sensing hairs of crickets. These structures are intended to be driven by viscous forces in the flow. Adapted from Dagamseh *et al.* (2010).

Because the cavity in the chip as used in the present approach is a primary feature of widely-produced silicon microphones, we anticipate that the sensing concept considered here could be implemented without a substantial departure from existing fabrication processes.

The idealized model of the cavity presented in the following contains only two design parameters, the length, L, and the depth, D, as shown in Fig. 3(a). These two parameters along with the acoustic wave number (the ratio of frequency to sound speed, $k = \omega/c$) are the only parameters in the model. With so few parameters we should hope the final equations in the model to be relatively simple and fairly easy to interpret.

The final result provides a remarkably simple approximate expression giving the ratio of the acoustic particle velocities flowing into and out of the cavity relative to the acoustic particle velocity one would see in an ideal plane traveling sound wave. The expression contains just two terms, one giving the differential flow into and out of the cavity which depends on the ratio of the cavity length L to the depth D. This differential flow is what one would expect if the fluid were incompressible since it does not involve any compression of the air within the volume. The second term gives the net flow which does involve compression of air in the volume. This term depends on the cavity depth and the acoustic wave number (i.e., the frequency and sound speed). The two terms readily provide the ability to determine the length and depth of the cavity required to achieve any of the well-known first-order directivity patterns, cardioid, omnidirectional, bidirectional etc.

In addition to our highly simplified model, the acoustic flow into and out of the opening of the cavity is detected experimentally using electro-spun nanofiber meshes which move with nearly the same velocity as the air and their velocity can be measured using a laser vibrometer. The use of thin fiber to examine acoustic particle velocity follows from earlier work by two of us on the sound-induced motion of spider silk (Zhou *et al.*, 2018; Zhou and Miles, 2017). Results were obtained using cavities having two different

J. Acoust. Soc. Am. **157** (1), January 2025
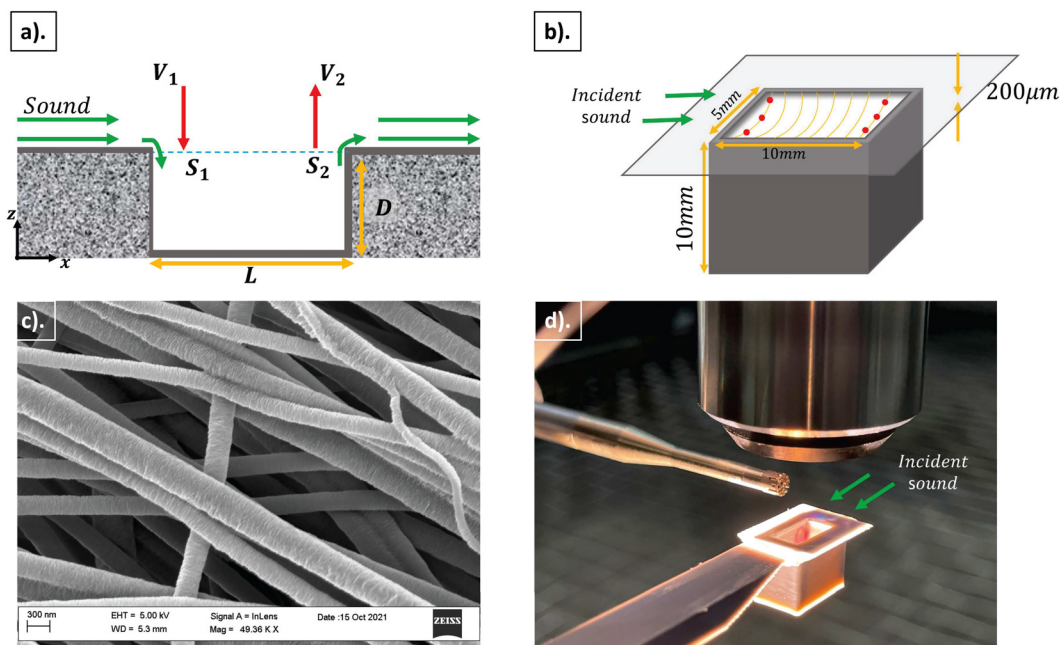
Lai *et al.*   31

FIG. 3. (Color online) Nanofiber mesh spun over the cavity. (a) 2D representation of the acoustic flow over and into a cavity. The cavity is divided in half with two equal open surfaces with areas S_1 and S_2. Air velocity is detected near the leading edge and the trailing edge as V_1 and V_2. As discussed in Sec. II, the cavity length L and depth D are important design parameters that determine the frequency range over which it permits simultaneous in and out flow as opposed to behaving as a conventional Helmholtz resonator. (b) Schematic of the large scale cavity. The top plate is 200μm thick. It has a rectangular opening 10 mm in length, and 5 mm in width. The top plate is placed over the cavity opening. Thin, flexible fibers were electro-spun over the opening of the top plate. Red dots indicate locations where the velocity of the fiber in the direction normal to the opening was measured. The large scale cavity has the dimensions of $L = 10$ mm, $D = 10$ mm. The opening of the cavity has the same dimension as the opening of the top plate. (c) SEM photo of the PVDF-TrFE electro-spun nanofibers. The average diameter of the fiber is 300 nm. (d) Experimental setup for measuring the acoustic response of the fiber mesh over the cavity showing the lens of the laser vibrometer to measure the fiber motion and the calibrated microphone to measure the incident sound pressure.

sizes. The "large-scale" cavity had dimensions 10 mm deep, 10 mm long, and 5 mm wide. The "small-scale," or micro-scale cavity had dimensions 0.5 mm deep, 3.5 mm long, and 1.8 mm wide. The fibers placed over the opening can accurately represent the air velocity field at the opening of the cavity. Experimental results are found to be in excellent agreement with those predicted by the simplified model as well as those obtained by a more detailed finite element model. The agreement between experimental results and two very dissimilar modeling methods suggests that the essential features of the system have been adequately captured.

The results presented here indicate that an effective way to detect the acoustic particle velocity in a sound field is to create a sensor that detects the flow in the opening of a cavity, where the open surface is oriented parallel to the wave propagation direction. This surface and cavity could be constructed on a silicon chip having dimensions similar to those used to fabricate MEMS microphones. The acoustic flow into and out of a properly designed cavity can present an excellent approximation to the acoustic particle velocity in the far field. The construction of this system is readily adaptable to silicon microfabrication processes and presents an attractive alternative to previous design approaches consisting of a flow-sensing structure placed orthogonal to the silicon chip surface.

The acoustic flow into and out of a suitably designed cavity is remarkably similar to the observed motion of tympanal membranes in two species of parasitic flies, which have been shown to possess directional hearing (Miles *et al.*, 1995; Robert *et al.*, 1999). These tympana form the top surface of an enclosed air-filled cavity, not unlike the cavity examined here. It seems plausible that the acoustic flow in the air space behind these tympanal membranes may play a significant role in determining their directional tympanal response. If so, the design of bioinspired directional microphones should consider the effects of the air-filled cavity, which may lead to less dependence on the details of the diaphragm mechanical design.

The highly simplified model of the acoustic flow in the cavity is presented in the following section. The experimental methods and results of detecting the acoustic flow in cavities having two different sizes are then presented along with those obtained using a more detailed finite element model. This is then followed by a discussion and conclusions.

II. TWO-DIMENSIONAL (2D) ANALYTICAL MODEL

In the following, we will examine the sound field in air in a small, shallow hole, or cavity, in a rigid planar surface. The sound field within the cavity results from a sound wave in the region above the hole traveling in the direction parallel to the planar surface. The dimensions of the hole are assumed to be smaller than the sound wavelength. Our goal here is to create the simplest model that captures the most

32   J. Acoust. Soc. Am. **157** (1), January 2025

Lai *et al.*

important features of the sound field within the hole; a more detailed model will doubtless account for many other effects such as those due to viscosity along with the compressibility and inertia of the gas but these will be neglected here to avoid obscuring the first-order effects. As a result, this model is applicable only at the lower frequencies, below the resonant frequencies of the system. Because of these simplifications, the result provides simple guidance on the length, L, and depth, D, in which the acoustic particle velocity is likely to flow in at one end of the hole and out the other, rather than be dominated by flow in and out that tends to be uniform across the opening. Uniform flow across the entire opening is typically encountered in a conventional Helmholtz resonator. In this study, we are mainly interested in the case where the flows at the two ends of the hole are simultaneously in opposite directions. This out-of-phase flow can result in negligible change of mass (and density) of the gas within the hole and, for our purposes, the fluid can be considered to be incompressible.

In this simple model, we will consider the hole to be rectangular with a length, L, in the direction of sound propagation and a width, B. Assume that the sound pressure is constant across the width so there is no flow in that direction. Again, the dimensions of the hole are taken to be significantly smaller than the acoustic wavelength. In particular, the depth of the hole is small enough that the acoustic pressure is nearly independent of the distance from the bottom of the hole, z, as shown in Fig. 3(a). In addition, a plane wave propagating in the x-direction above the hole, as shown in Fig. 3(a) is not significantly affected by the hole. We can express the fluctuating sound pressure, $p(x, z, t)$, in this plane traveling wave propagating in the positive x direction as a function of x, z, and time, t as

$$p(x, z, t) = P e^{i\omega t} e^{-ikx}, \tag{1}$$

where $k = \omega/c$ is the wave number, ω is the frequency in rad/s, $i = \sqrt{-1}$, and c is the speed of acoustic wave propagation (Miles, 2020). Consider the opening of the hole to be divided into two regions having areas S_1 and S_2 as depicted in Fig. 3(a). These adjacent areas will be assumed to be equal but for now, denote them with subscripts 1 and 2. The centers of these areas will be separated by a distance $d = L/2$ where L is the total length of the cavity. Each area will be considered to have a width B and length $L/2$ so that $S_i = BL/2$ for $i = 1$, 2; the areas are taken to be equal, $S_1 = S_2 = S$.

In this highly simplified view of the cavity, consider the motion of the air in the two areas S_1 and S_2 to be in the vertical direction and uniform within each area, so that each of the two surfaces acts like a uniform, massless piston. This type of system can be modeled using the approach described in Miles (2016). Here, each of the two areas is considered to be a piston having no mass or stiffness connecting it to the substrate. Let the vertical displacement of these two imaginary membranes be x_1 and x_2. Each of these motions results in a change in pressure, P_v within the volume, V as given in Eq. (14) of Miles (2016), repeated here for convenience,

$$P_v = -\rho_o c^2 \Delta V / V = -\rho_o c^2 x_i S_i / V, \quad i = 1, 2, \tag{2}$$

where ρ_0 is the nominal air density. Let the depth of the back volume be D so that the total volume of air behind these imaginary diaphragms will be $V = LDB$. Note that an outward displacement, x_i results in an increase in the total volume and a reduction in the internal pressure. Equation (19) of Miles (2016) gives the force applied to diaphragm j due to the compression of the air in the back volume resulting from the displacements, x_i of N diaphragms that share a common back volume,

$$-P_j S_j = k_j x_j + S_j \sum_{i=1}^{N} x_i S_i \rho_o c^2 / V, \quad j = 1, ..., N. \tag{3}$$

In our case, since our imaginary diaphragms have no mechanical stiffness, k_j, we will neglect $k_j x_j$.

If there are only two areas, Eq. (3) becomes

$$-P_1 S_1 = S_1 \sum_{i=1}^{2} x_i S_i \rho_o c^2 / V,$$
$$-P_2 S_2 = S_2 \sum_{i=1}^{2} x_i S_i \rho_o c^2 / V, \tag{4}$$

where, again, the mechanical stiffness terms, k_j in Eq. (3) have been neglected.

The net force from the external sound field given in Eq. (1) and the force due to the air in the back volume in Eq. (3) must equal the rate of change of the momentum of the total moving mass, composed of the air within the volume. Because our system has two coordinates, x_1 and x_2, it is helpful to express the kinetic energy in terms of these coordinates, or some linear combination of them. Consider the energy and momentum due to the difference between them, $\dot{x}_2 - \dot{x}_1$. The total volume of air within the back volume, $V = LDB$, will have a mass given by $\rho_0 LDB$. This mass of air will be assumed to move with a uniform velocity within the volume due to the difference in the membrane velocities. The momentum of this mass may be estimated by $\rho_0 LDB(\dot{x}_2 - \dot{x}_1)$. The kinetic energy of this mass will be

$$T_{diff} = \frac{1}{2} \rho_0 V (\dot{x}_2 - \dot{x}_1)^2. \tag{5}$$

This expression for the kinetic energy can provide a convenient way to express the rate of change of momentum associated with each coordinate, x_1 and x_2. The rate of change of momentum must balance the net force. Let the forces applied to each area by the external field [Eq. (1)] be f_{e_1} and f_{e_2}. The net force applied to each area, including that due to the external sound field, must equal the rate of change of momentum associated with each coordinate,

$$f_{e_1} = S_1 \sum_{i=1}^{2} x_i S_i \rho_o c^2 / V + \rho_0 V(\ddot{x}_1 - \ddot{x}_2),$$
$$f_{e_2} = S_2 \sum_{i=1}^{2} x_i S_i \rho_o c^2 / V + \rho_0 V(\ddot{x}_2 - \ddot{x}_1). \tag{6}$$

J. Acoust. Soc. Am. **157** (1), January 2025

Lai *et al.*   33

Equation (6) can be expressed in matrix form as

$$K\begin{bmatrix} 1 & 1 \\ 1 & 1 \end{bmatrix}\begin{pmatrix} x_1 \\ x_2 \end{pmatrix} + \rho_0 V\begin{bmatrix} 1 & -1 \\ -1 & 1 \end{bmatrix}\begin{pmatrix} \ddot{x}_1 \\ \ddot{x}_2 \end{pmatrix} = \begin{pmatrix} f_{e_1} \\ f_{e_2} \end{pmatrix}, \quad (7)$$

where

$$K = S^2\rho_o c^2/V. \quad (8)$$

We have simplified things by taking $S_1 = S_2 = S$. As mentioned previously, the centers of the two areas are separated by a distance $d = L/2$. The sound field is assumed to be a plane wave propagating in the x direction, with the origin $x = 0$ at the midpoint of the cavity. Let the two pressures at the centers of the two areas be P_1 and P_2, where

$$P_1(t) = Pe^{i\omega t + ikd/2} \quad \text{and} \quad P_2(t) = Pe^{i\omega t - ikd/2}. \quad (9)$$

Equation (7) depends on forces instead of pressures and since we have assumed the areas are equal, the two forces are

$$f_{e1}(t) = PSe^{i\omega t + ikd/2} \quad \text{and} \quad f_{e2}(t) = PSe^{i\omega t - ikd/2}. \quad (10)$$

The particular solution to Eq. (7) can be written as

$$\begin{pmatrix} x_1(t) \\ x_2(t) \end{pmatrix} = e^{i\omega t}\begin{pmatrix} X_1 \\ X_2 \end{pmatrix}, \quad (11)$$

where X_1 and X_2 are complex amplitudes. Equations (7), (10), and (11) lead to

$$\begin{pmatrix} X_1 \\ X_2 \end{pmatrix} = \left\{ K\begin{bmatrix} 1 & 1 \\ 1 & 1 \end{bmatrix} - \omega^2\rho_0 V\begin{bmatrix} 1 & -1 \\ -1 & 1 \end{bmatrix} \right\}^{-1}$$
$$\times \begin{pmatrix} PSe^{ikd/2} \\ PSe^{-ikd/2} \end{pmatrix}. \quad (12)$$

It is helpful to express our solution in terms of velocity rather than displacement. The velocities of our surfaces are

$$\begin{pmatrix} v_1(t) \\ v_2(t) \end{pmatrix} = e^{i\omega t}\begin{pmatrix} V_1 \\ V_2 \end{pmatrix} = i\omega\begin{pmatrix} x_1(t) \\ x_2(t) \end{pmatrix}, \quad (13)$$

where $V_1 = i\omega X_1$ and $V_2 = i\omega X_2$ are complex velocity amplitudes.

In addition, we'd like to normalize them as the ratio of each velocity to the velocity of the acoustic particles in a plane sound wave. The acoustic particle velocity in an ideal plane sound wave is

$$V_{air} = \frac{P}{\rho_0 c}. \quad (14)$$

The normalized velocities of our surfaces are then

$$\begin{pmatrix} V_1/V_{air} \\ V_2/V_{air} \end{pmatrix} = i\omega\left\{ K\begin{bmatrix} 1 & 1 \\ 1 & 1 \end{bmatrix} - \omega^2\rho_0 V\begin{bmatrix} 1 & -1 \\ -1 & 1 \end{bmatrix} \right\}^{-1}$$
$$\times \begin{pmatrix} \rho_0 cSe^{ikd/2} \\ \rho_0 cSe^{-ikd/2} \end{pmatrix}. \quad (15)$$

The algebra may be simplified a bit by letting

$$\lambda = \frac{\omega^2\rho_0 V}{K} = \left(\frac{\omega}{c}\right)^2 4D^2 = 4(kD)^2, \quad (16)$$

where, again, $k = \omega/c$ is the wave number and D is the cavity depth as shown in Fig. 3(a). Equation (15) becomes

$$\begin{pmatrix} V_1/V_{air} \\ V_2/V_{air} \end{pmatrix} = i\omega\left\{ \begin{bmatrix} 1 & 1 \\ 1 & 1 \end{bmatrix} - \lambda\begin{bmatrix} 1 & -1 \\ -1 & 1 \end{bmatrix} \right\}^{-1}$$
$$\times \begin{pmatrix} \rho_0 cS/Ke^{ikd/2} \\ \rho_0 cS/Ke^{-ikd/2} \end{pmatrix}. \quad (17)$$

Inverting the matrix and rearranging give

$$\begin{pmatrix} V_1/V_{air} \\ V_2/V_{air} \end{pmatrix}$$
$$= \frac{-i\omega\rho_0 cS}{4K\lambda}\begin{bmatrix} 1-\lambda & -1-\lambda \\ -1-\lambda & 1-\lambda \end{bmatrix}\begin{pmatrix} e^{ikd/2} \\ e^{-ikd/2} \end{pmatrix}$$
$$= \frac{-i\omega\rho_0 cS}{4K\lambda}\begin{pmatrix} (1-\lambda)e^{ikd/2} - (1+\lambda)e^{-ikd/2} \\ -(1+\lambda)e^{ikd/2} + (1-\lambda)e^{-ikd/2} \end{pmatrix}. \quad (18)$$

Using Eq. (16), Eq. (18) becomes

$$\begin{pmatrix} V_1/V_{air} \\ V_2/V_{air} \end{pmatrix} = \frac{-ic}{8D\omega}\begin{pmatrix} (1-\lambda)e^{ikd/2} - (1+\lambda)e^{-ikd/2} \\ -(1+\lambda)e^{ikd/2} + (1-\lambda)e^{-ikd/2} \end{pmatrix}, \quad (19)$$

where we have used the fact that

$$\frac{S}{V} = \frac{1}{2D}. \quad (20)$$

Equation (19) may also be written as

$$\begin{pmatrix} V_1/V_{air} \\ V_2/V_{air} \end{pmatrix} = \frac{-ic}{8D\omega}\begin{pmatrix} 2i\sin(kd/2) - 2\lambda\cos(kd/2) \\ -2i\sin(kd/2) - 2\lambda\cos(kd/2) \end{pmatrix}$$
$$= \begin{pmatrix} \dfrac{1}{4Dk}\sin(kd/2) + ikD\cos(kd/2) \\ -\dfrac{1}{4Dk}\sin(kd/2) + ikD\cos(kd/2) \end{pmatrix}. \quad (21)$$

When $kd/2 \ll 1$, this can be approximated by

$$\begin{pmatrix} V_1/V_{air} \\ V_2/V_{air} \end{pmatrix} \approx \begin{pmatrix} \dfrac{d}{8D} + ikD \\ -\dfrac{d}{8D} + ikD \end{pmatrix} = \begin{pmatrix} \dfrac{L}{16D} + ikD \\ -\dfrac{L}{16D} + ikD \end{pmatrix}. \tag{22}$$

Equation (22) provides a remarkably simple way to determine the necessary length and depth of a cavity (or a back-side hole) to achieve either omnidirectional or first-order directional response. We can account for the effects of a plane sound wave incident at an angle ϕ relative to the x direction, i.e., the long axis of the cavity shown in Fig. 3(a), by replacing the wave number k by $k\cos(\phi)$. Equation (22) then reduces to the cardioid directivity pattern when the in-phase and out-of-phase terms have identical amplitudes. This occurs at a frequency given by

$$\omega_c = \frac{Lc}{16D^2}. \tag{23}$$

At frequencies below ω_c, we expect out-of-phase, bidirectional response while at higher frequencies we expect in-phase, omnidirectional response. As an example, if the length of the cavity is $L = 1\,$mm and the depth is $D = 0.5\,$mm, this gives $\omega_c \approx 86\,000$ rad/s or 13 687 Hz. Below this frequency, the in-and-out flow of air in the sound field essentially provides a means of estimating the acoustic particle velocity in the plane sound wave. At higher frequencies, or where the depth of the cavity becomes large enough relative to the sound wavelength, the dominant motion is essentially uniform across the opening with the air flowing in and out with the fluctuating pressure. In other words, at higher frequencies, it behaves more like a conventional Helmholtz resonator.

III. MEASUREMENT OF ACOUSTIC FLOW IN CAVITIES

In order to better-understand the acoustic flow into and out of small cavities, measurements have been performed using both "large-scale" and "micro-scale" cavities. Because our interest here is on acoustic sensing, our "large scale" cavity is not particularly large, having dimensions on the order of millimeters so that the dimensions are reasonably small relative to acoustic wavelengths in the audible range of frequencies. In the following, experimental methods and results are presented for both types of cavities. These results are then compared to those obtained from our simplified analytical model presented previously along with results obtained from a detailed finite element model.

All acoustic measurements were conducted in the anechoic chamber at Binghamton University. The chamber interior dimensions are 4.2 m wide, 5.4 m long, and 3.2 m tall. The absorbent wedges covering all surfaces are made of fiberglass. The chamber has been certified by the manufacturer to provide an anechoic environment at all frequencies above 80 Hz. The noise floor of the chamber is approximately 0 dBA. The anechoic chamber was tested using methods specified in: ISO Standard 3745-2003, Annex A,

"General procedures for qualification of anechoic and hemi-anechoic rooms." The primary components of the measurement system were a data acquisition system (NI PXI 1033, National Instruments, Austin, TX), a laser vibrometer (Polytec OFV 534, Polytec, Baden, Germany), a fixture for the cavity, a loudspeaker system, a reference microphone (B&K 1/8 in. reference microphone, B&K, Naerum, Denmark), and a motorized positioning system (Newport).

The acoustic domain examined here consists of either the "large scale" or "micro-scale" rectangular cavity having one side open as shown in Fig. 3. Measurements of the air particle velocity in the direction normal to the open surface were obtained at several locations across the opening of each cavity while a plane acoustic wave traveled parallel to the open surface in the domain outside each cavity.

A. Experimental methods: Large scale cavity

Figure 3(b) shows a schematic of the apparatus used to measure the air particle velocity in the "large scale" cavity. The top plate shown in the figure, having a thickness of $200\,\mu$m, is placed over the cavity opening. Thin, flexible fibers were electro-spun over the opening of the plate, as described in the following. The sound-induced motions of the fibers were measured using a laser vibrometer to detect the flow of the air at the top surface. The plate with fibers could then be placed over cavities having different depths, allowing the same set of fibers to be used to investigate the flow in different cavities. The top plate and the "large scale" cavity on which it was placed were fabricated via fused deposition modeling (FDM) three-dimensional (3D) printing technology employing an Anycubic Kobra Plus 3D printer. Poly(lactic acid) (PLA) filament was utilized as the printing material with an infill density of 40%.

The top plate used for this "large scale" cavity featured a hole measuring 10 mm in length, 5 mm in width, and $200\,\mu$m in depth. The plate was used to measure the flow into and out of two different cavities that shared the same length and width dimensions but differed in depth, measuring 5 and 10 mm, respectively.

To collect highly-aligned electrospun Poly(vinylidene fluoride-trifluoroethylene) (PVDF-TrFE) fibers across the top plate, two strips of copper tape were attached to the long-edge of the hole in the top plate, comprising parallel electrodes. PVDF-TrFE solution (16 wt.%) was prepared by dissolving PVDF-TrFE powders (75/25, PolyK Technologies, LLC, North Philipsburg, PA) in a solvent mixture of dimethylformamide (Carolina Chemical) and acetone (VWR Chemicals) in a 3:2 volume ratio. This solution was thoroughly mixed overnight at ambient temperature using a vortex mixer (Daigger Scientific Inc., Buffalo Grove, IL). The homogeneous PVDF-TrFE solution was then loaded into a plastic syringe with a metal needle (22 gauge) connected via a Teflon tube. A syringe pump was employed to control the flow rate at 0.1 ml/h. The blunt needle and the 3D printed top plate with parallel electrodes on the long-edge sides of the hole were mounted on a 3-axis

J. Acoust. Soc. Am. **157** (1), January 2025

Lai *et al.*   35

robot (JANOME JR3304, Tokyo, Japan) to precisely control the fiber deposition across the hole on the top plate by restricting electrospinning duration to 1 s and regulating travel distance of the blunt needle to 20 mm. The distance between the metal needle tip and the grounded collector was maintained at 20 mm. A 4 kV voltage was applied to the metal needle using a high-voltage power supply (Acopian Technical Company, Easton, PA). The entire fiber fabrication process was conducted under room temperature conditions.

The fiber mesh was coarsely spun on the top plate which was placed on the open surface of the cavity. The fiber mesh was then located at the cavity opening. Since the average fiber diameter is approximately 300 nm, when woven to form a mesh with minimal tension it is compliant enough to move with the air, much like the spider web moving due to sound (Zhou et al., 2022; Zhou and Miles, 2017). The laser was focused on the fiber mesh to measure the fiber motion in the direction normal to the cavity opening, i.e., parallel to the laser beam. Fiber velocity due to sound was measured at the locations of the red dots shown in Fig. 3(b). The reference microphone was placed near the opening of the cavity to measure the incident sound pressure as shown in Fig. 3(d). The excitation consisted of a stepped sinusoidal

signal and time-domain windowing was used to acquire the acoustical frequency response while eliminating the acoustical reflection and uncorrelated noise (Lai et al., 2022).

B. Experimental results: Large scale cavity

To examine the acoustic flow into and out of the large scale cavity, we attempted to measure the influence of the cavity on the acoustic flow field. To do this, we first measured the fiber mesh motion in the hole of the thin top plate shown in Fig. 3(b), without the cavity beneath it. Because the 200 μm thickness of the top plate was considerably smaller than the sound wavelength at frequencies of interest here, it was too thin to influence the sound field when placed in parallel with the direction of sound propagation. The data shown in Fig. 4(c), especially the phase, show that there is little correlation in the flow in the direction into and out of the holes in the top plate between the near side and far side. Figure 4(d) shows the measured normalized velocity and phase of the acoustic particle velocity at each end of the hole in the top plate when the cavity is in place. In this case, the phase data show the velocities of the fibers at the near and far ends of the cavity tend to be in opposite directions, while the normalized velocity, V/V_{air} shows the amplitudes
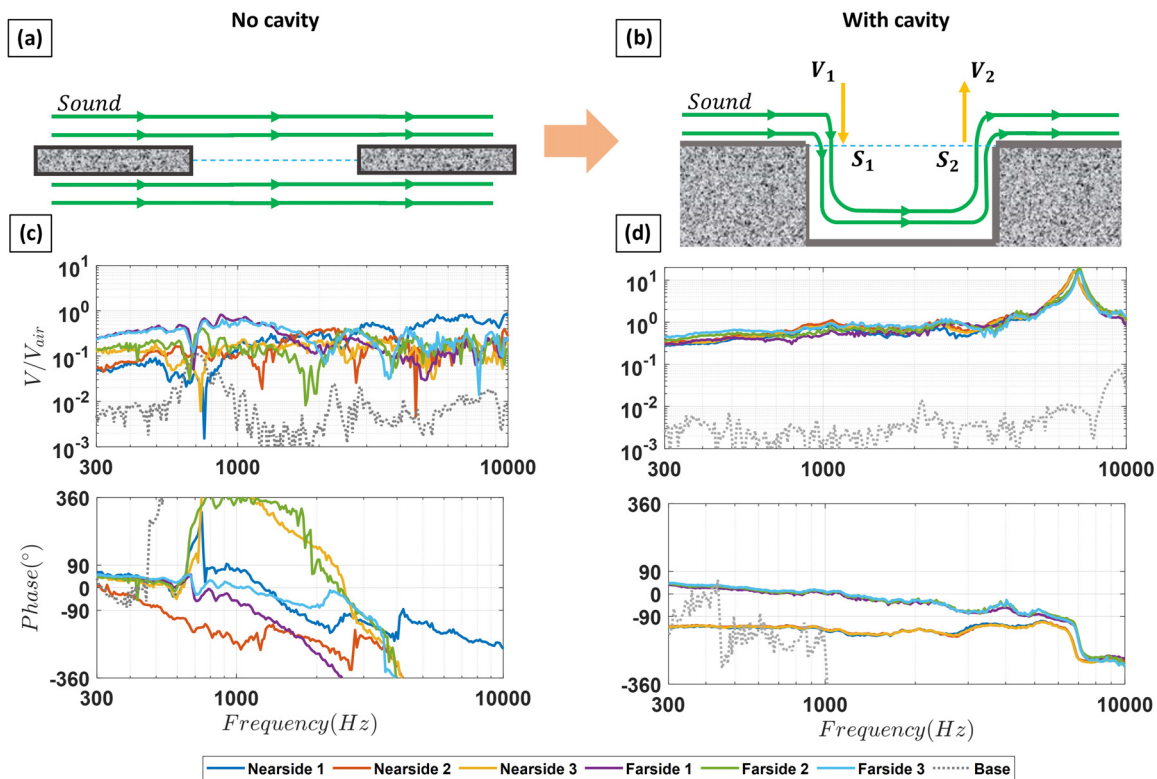

FIG. 4. (Color online) Acoustic flow field comparison with and without the cavity. Here, (a) and (b) show a 2D representation of the acoustic flow due to a plane wave traveling parallel to the plane of the plate without and with the cavity, respectively; (c) and (d) show the normalized acoustic particle velocity of the air in the direction perpendicular to the cavities open surface obtained by measuring the fiber mesh velocity near the surface of the cavity. Data are shown for three locations equally spaced across the width of the cavity opening at both the near and far ends of the cavity. These measurements are thus obtained at locations that are close to the leading and trailing edges of the cavity. The results are normalized relative to the acoustic particle velocity in the far field, away from the cavity. The measured results show that when the cavity is present the measured phase between the leading and trailing edges differ by approximately 180 degrees across a wide frequency range; the sound thus flows into the cavity on one end while flowing outward from the cavity at the other end.
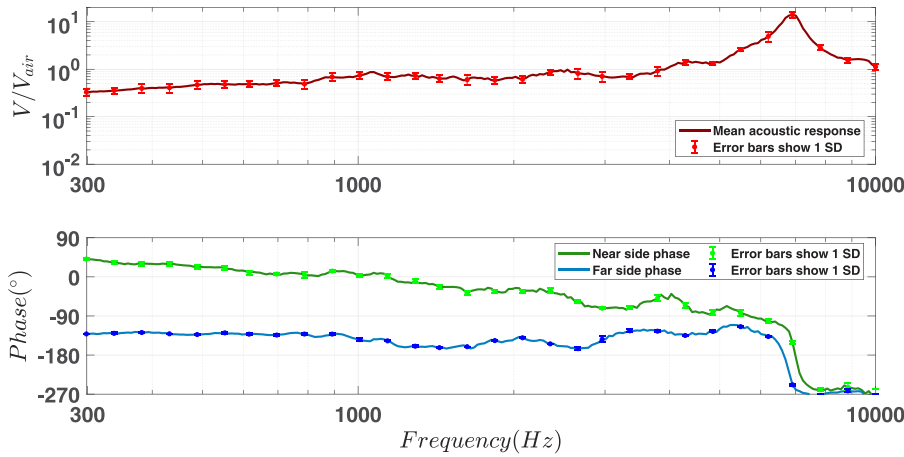
FIG. 5. (Color online) Statistical analysis of the acoustic response data measured using the large scale cavity model. The solid lines are calculated mean values of the acoustic response magnitude and phase. The error bars show 1 standard deviation (SD). As in Fig. 4, data are shown for three locations equally spaced across the cavity width at both the near and far ends of the cavity. The magnitude plot showing V/V_{air} shows the mean of all of the data of both ends of the cavity, which are all in close agreement. The phase shows that the flow at the two ends is nearly out of phase. The normalized velocities, V/V_{air}, at both edges are in close agreement.

are nearly identical. The air thus flows into the cavity on the near side as it flows out of the cavity on the far side. According to the analytical model in Eqs. (21) and (22), the out-of-phase fiber mesh motions on the near and far side will vary with frequency, ω. Again, recall that the wave number is $k = \omega/c$ where c is the sound propagation speed. Since the depth of the cavity is 10 mm, a resonance is expected at approximately 7 kHz. The data shown in Fig. 4(d) confirm our expectations.

The amplitudes of the normalized velocities are nearly all the same and are nearly equal to unity over a wide range of frequencies as shown in Fig. 5. In addition, the phase between the near and far sides is close to 180 degrees over a fairly broad frequency range; the air particle velocity due to sound is moving in opposite directions in and out of the cavity at frequencies up to the first resonant frequency, approximately 7 kHz.

To examine the influence of the depth of the cavity, measurements were obtained with the cavity depth reduced from 10 to 5 mm. The resulting averaged frequency response and phase are compared in Fig. 6. Reducing the depth of the cavity by a factor of two resulted in the resonance frequency being doubled; the frequency region where the flow is out of phase is expanded from about 7 to approximately 14 kHz.

Because the vast majority of microphones are fabricated at the micro-scale, to be consistent with typical portable electronic devices, micro-scale cavities have also been examined. The methods and results are presented in the following.

C. Experimental methods: Micro-scale cavity

The silicon micro-scale cavity is fabricated at the Cornell NanoScale Science and Technology Facility in Ithaca, NY. The cavity is fabricated on a 4.5 by 3.5 mm chip by etching a rectangular through-hole in the center. In our experiments, the bottom of the hole is closed by placing the chip on a glass slide, or similar solid, smooth surface. The hole size is 3.5 by 1.8 mm with a depth of 0.5 mm, equal to the wafer (and chip) thickness. The wavelength of sound at the upper limit of typical human hearing (20 kHz) is approximately $\lambda \approx c/f = 344/20\,000 = 17.2$ mm, significantly larger than the cavity dimensions so we do not expect resonances to significantly affect the results. In addition, we expect the out-of-phase air motion at the two ends to have a much wider frequency range than was observed for the large-scale cavity discussed before. As with the larger scale cavity, PVDF nanofibers were electro-spun on the cavity opening on the surface of the chip. The mesh density is controlled to be very low so the air can travel between the fibers and each fiber can fully interact with the air motion. The
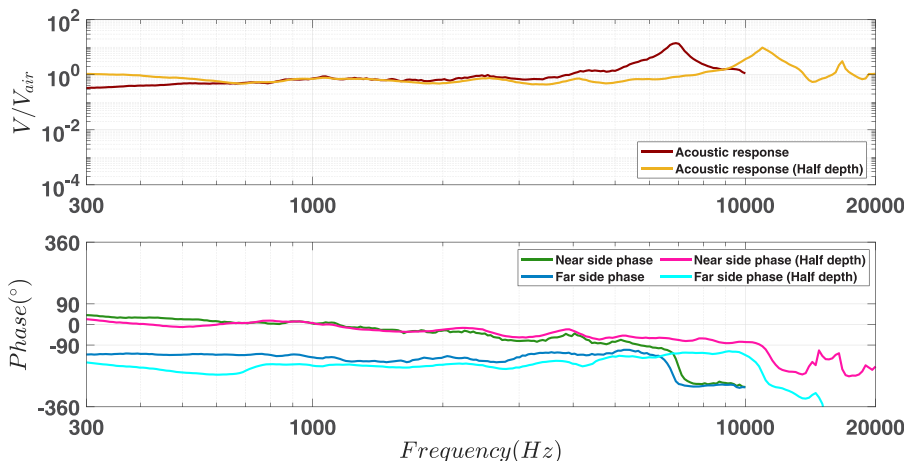

FIG. 6. (Color online) Reducing the cavity depth increases the resonant frequency. Results are shown for the original, full depth cavity and when the cavity depth is reduced by a factor of two. With the cavity depth cut in half, according to the analytical model of Sec. II, the resonance frequency of this second order Helmholtz resonator will double. The phase separation between the near side and far side, or leading and trailing edges, will also shift with the resonance frequency. The measured data are consistent with these predictions.
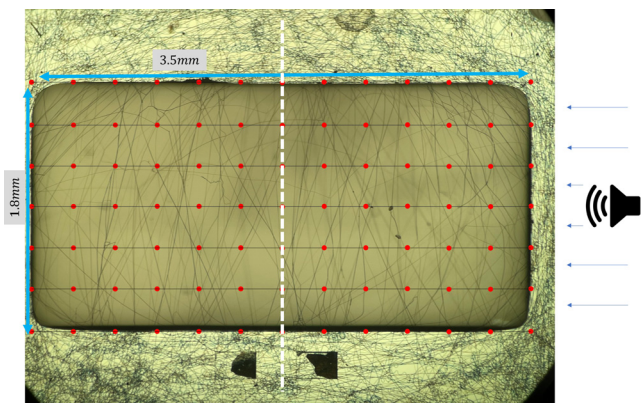
FIG. 7. (Color online) Measuring scheme of the micro fabricated cavity with nanofiber mesh spun over the opening surface. The cavity measures 3.5 by 1.8 mm. A plane sound wave is incident from the right. Red dots indicate the laser measuring locations. The laser is focused on the individual fiber that is closest to each measurement location. The dashed line is the middle line that divides the cavity into two equal regions. The nanofiber mesh is uniformly spun over the cavity opening.

measurement locations are illustrated in Fig. 7. The outer perimeter of the pattern defines the measurements on the chip top surface. The central vertical line on the fiber mesh is indicated by the white dashed line. This line contains five equally spaced measurement locations. The rest of the measured locations are divided into five rows. The incident sound comes from the right side as indicated by the loudspeaker depicted in Fig. 7. The leading edge is considered as the side nearest to the loudspeaker, while the trailing edge is considered as the side opposite the loudspeaker.

D. Experimental results: Micro-scale cavity

The frequency responses of the fiber mesh over the micro-scale cavity are shown in Fig. 8. Again, the amplitude of the velocity is normalized relative to that of the acoustic particle velocity in the far-field. At distances sufficiently far from the cavity, the sound is essentially unaffected by the presence of the cavity. The figure represents results obtained at the array of locations shown in Fig. 7. The figure shows that the predicted amplitude and phase of the acoustic

particle velocities on each end of the cavity, as predicted by Eq. (21), are in very close agreement with the measured results.

A rather wide range of measured amplitudes are shown in the upper panel of Fig. 8 while the phase data are generally either ±90 degrees relative to the acoustic particle velocity of a plane wave. The variation in measured particle velocity amplitude can be better understood by considering the variation of the amplitude with location. Because the results shown in Fig. 8 do not vary significantly with frequency, it may be instructive to consider how the velocity varies with position at a representative frequency.

To better illustrate how the measured velocity varies with position, the normalized response obtained at all measured locations shown in Fig. 8 are shown for a number of frequencies in 3D plots in Fig. 9. To increase our confidence in the experimental methods, results have also been obtained using the finite element method (COMSOL). The model predicts the flow in the cavity due to an incident plane acoustic wave as in the experiment and accounts for the effects of compressibility and viscosity. The model does not, however, include the effects of the fibers, which were intended to have minimal influence on the acoustic flow. Because of the diminutive size of the cavity, the numerical results include the influence of viscosity on the acoustic flow. The numerical results are shown in Fig. 10. The measurements shown in Fig. 9 show the out-of-phase motion at the two ends of the cavity, in agreement with the predicted results shown in Fig. 10.

IV. DISCUSSION AND CONCLUSIONS

As mentioned in Sec. I, a major motivation for this study has been to explore a method of constructing an acoustic particle velocity sensor that presents only a modest departure from the fabrication process used to create current MEMS microphones. Our present focus has been more on how to position or package the sensing element than on how to design the sensing structure itself. Previous efforts have employed structures that protrude from a planar substrate, much like insect flow-sensing hairs. While this can be an effective approach and obviously endorsed by Nature, it
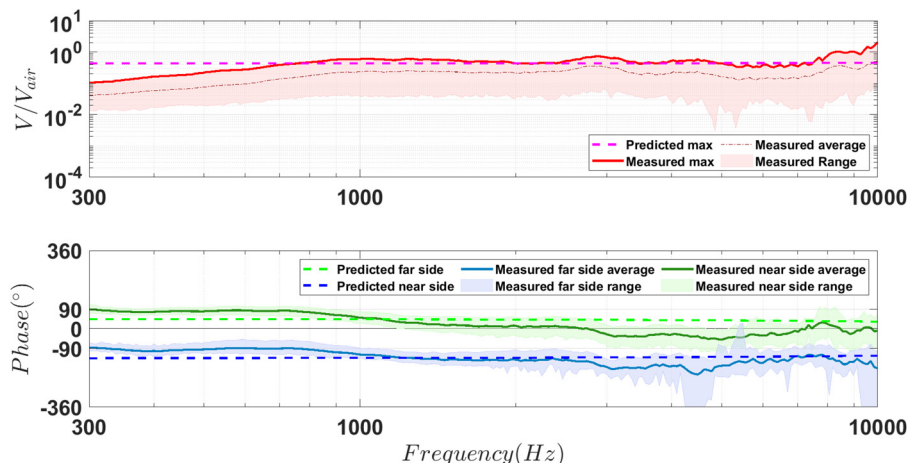

FIG. 8. (Color online) Measured acoustic response of the micro-scale cavity model. The solid red line shows the measured maximum response presumably at both edges. The dashed lines show the predicted response and phase at the edges by the analytical model. The area plots show the variation of the data set.
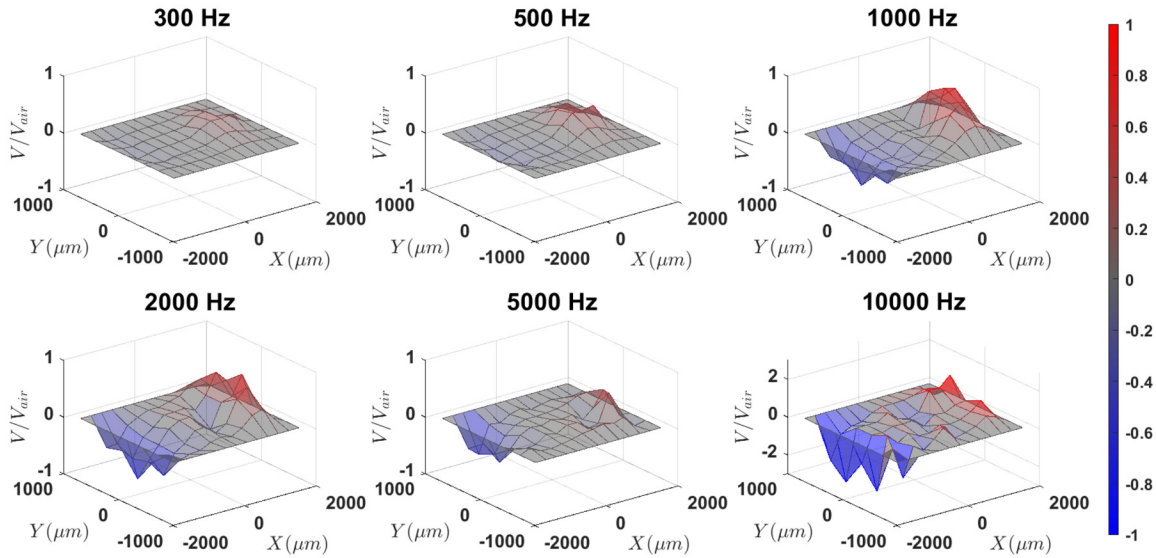
FIG. 9. (Color online) 3D visualization of the measured acoustic fiber motion due to flow in and out of the cavity at 300, 500, 1000, 2000, 5000, 10 000 Hz. The measured results indicate that the sound-driven flow is both into and out of the cavity at each end, as predicted by the analytical model of Eq. (22). Air particles will flow into the cavity from the leading edge and flow out from the trailing edge due to acoustic traveling wave. Below the lowest mode of the cavity, the air acts incompressible. The same amount of air that flows into the cavity also flows out of the cavity at the other end.

leads to a structure that requires a dramatic departure from standard silicon microfabrication processes. In addition, the sensing element is exposed to non-acoustic forces along with the desired sound. It is also vulnerable to damage. Our aim has been to explore other, more practical, and we hope, more effective ways to package an acoustic flow-sensing device.

The approach taken in this study is to first consider the use of a silicon chip, which is, of course, the essential component in MEMS microphones. These microphones also typically require a through-hole to be etched into the silicon chip. The first step in designing either a pressure-sensing microphone or a flow-velocity sensing microphone should be to carefully determine the proper dimensions of this air

space behind the sensing structure. In conventional pressure-sensing microphones, the sound pressure is sensed by detecting the deformation of a pressure-sensing diaphragm over an opening of the hole. The primary aim of the present study is then to examine the sound-driven flow in the cavity as the first step in designing a flow-sensing microphone. Our hope is that this approach will lead to a flow-sensing microphone that represents a minimal alteration of existing pressure-sensing microphone designs.

The focus of the present study is on the use of the cavity to facilitate acoustic flow sensing; we will address the design of a viscous acoustic flow-sensing structure in a future effort. Our eventual aim is to detect acoustic flow velocity using a viscous-driven structure, such as a
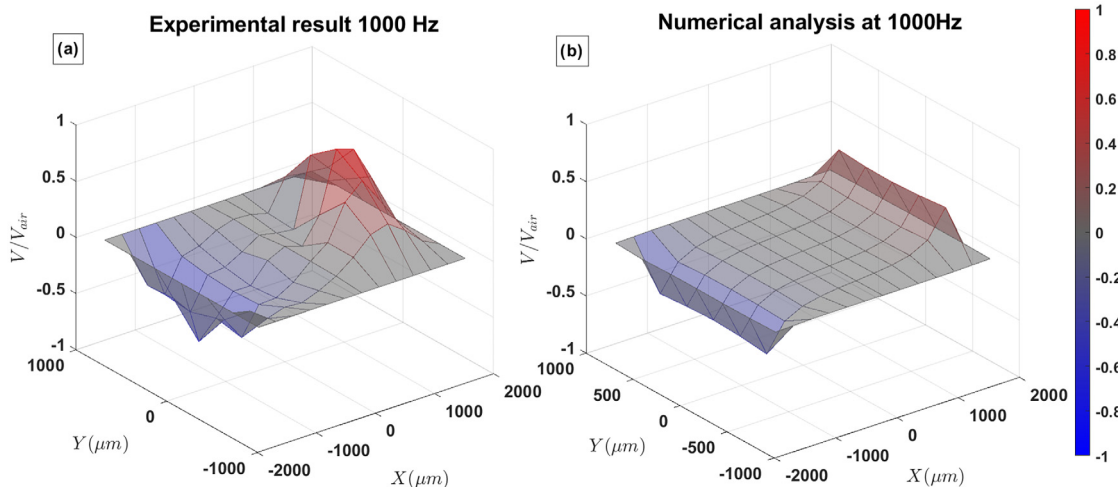

FIG. 10. (Color online) Flow velocity predicted by our COMSOL model is similar to our measured results. (a) Measured flow velocity at 1000 Hz from Fig. 9(a). (b) 3D visualization of the COMSOL simulated acoustic particle motion at 1000 Hz. These predicted results account for the effects of viscosity and compressibility of the air in the cavity.

J. Acoust. Soc. Am. **157** (1), January 2025

Lai *et al.*   39

compliant microbeam, at the opening of the hole rather than a pressure-sensitive diaphragm. A properly designed hole or cavity will essentially re-direct the acoustic flow from the direction parallel to the plane of the chip top surface so that the air flows into and out of the hole due to sound. Detecting that in-and-out flow could be accomplished with sensing structures that are fabricated **parallel** to the surface of the chip, as is done when fabricating silicon microphone diaphragms and countless other MEMS devices. If the acoustic flow velocity into and out of the chip is reasonably similar to the acoustic flow velocity in the free stream, then this system could comprise the essentials of a MEMS flow-sensing microphone fabricated with nearly the same steps that have already been established for making MEMS microphones.

It should be noted that the acoustic particle velocity exists because of spatial pressure gradients in the sound field. So, if we create a device that detects pressure gradients through the use of a diaphragm or membrane acted on by the pressures that are normal to its two opposing surfaces, then its resulting motion can be expected to correspond with the motion of the acoustic particles. An alternative way to detect the motion of the acoustic medium could be to devise a structure that is acted on directly by the flow rather than the pressure gradient that causes the flow. This could be realized using a thin hair or fiber driven by viscous forces resulting from the relative motion between the pressure-gradient-driven flow and the solid hair or fiber.

Viscous forces are employed in ears that use fine hair to sense the sound. These two approaches, pressure gradients versus viscous forces, require very different sensor designs and sizes; pressure gradients are most easily detected using a membrane or diaphragm-like structure while viscosity-driven structures normally take the form of relatively small, fine hairs, thin beams, or fibers. In the following we will refer to either type of sensor to be directional since both quantities, pressure gradient or flow velocity, are vectors having both magnitude and direction.

Again, our current focus is not on the design of the sensing structures themselves but on the design of a cavity used to support and contain the sensing structures. The inspiration for the use of a cavity to facilitate the use of viscous-driven acoustic flow sensors is inspired by methods used to detect sound pressure gradients by small animals. Animals often need to detect the direction of sound propagation. This is achieved by sensing the sound pressure gradient through the use of a pair of ears rather than sensing only the scalar pressure alone, as could be accomplished using a single ear. Nearly all animals that sense sound pressure do so with more than one ear.

Some small animals have evolved coupled pressure-sensing ears that enable the detection of the pressure gradient on their external surfaces and hence, the direction of acoustic propagation despite their small size (Knudsen, 1980; Larsen *et al.*, 2016; Michelsen *et al.*, 1994; Robert, 2005). There are numerous examples of other acoustically coupled ears, where the air spaces behind the tympana are connected by an air-filled tube or duct (Fletcher and Hill,

1978; Mason, 2016; Vossen *et al.*, 2010). In the parasitoid fly, *Ormia ochracea*, the tympanal ears are coupled by a cuticular bridge which has been identified as crucial to enabling it to localize sound remarkably well (Miles *et al.*, 1995). In this animal, the detection of differences in pressure at the two tympana along with the detection of the common, or spatial average pressures produces a directionally dependent tympanal response; the ear that is closest to a sound source responds with significantly more amplitude than the opposite ear, which is a mere fraction of a millimeter further from the sound source.

The discovery of the coupled tympana of *Ormia ochracea* continues to result in numerous efforts at biomimicry to create miniature directional microphones (Ando *et al.*, 2009; Bauer *et al.*, 2016, 2017; Cui *et al.*, 2006; Ishfaque and Kim, 2017; Liu *et al.*, 2008; Miles and Hoy, 2006; Miles *et al.*, 2009; Rahaman and Kim, 2019, 2020a,b; Sung *et al.*, 2007; Zhang *et al.*, 2018; Zhang *et al.*, 2017; Zhang *et al.*, 2014). A primary challenge in these designs has been to create a light-weight, pressure-sensing structure that responds well to pressure gradients. Although not addressed in most of these biomimetic designs, a daunting challenge in creating small directional microphones is to faithfully capture the sound field while minimizing the response to random thermal noise (Lai *et al.*, 2024).

Along with *Ormia*, another parasitoid fly *Emblemasoma spp.* has shown directional tympanal hearing (Robert *et al.*, 1999). In this case, however, the pair of tympana connected by an intertympanal bridge in *Ormia* are replaced by a **single** tympanal membrane having two sets of sensory cells; essentially a single tympanum shared by two ears. The fact that the tympanal structures of these two flies, *Ormia* and *Emblemasoma*, have very different tympanal structures while both achieve directional tympanal response suggests that the structure of the tympana may not be the only determining characteristic of these ears that enables directional hearing; other anatomical features of these ears might be utilized in creating biologically-inspired designs of directional acoustic sensors.

In both of these flies, the tympana encloses a common back volume of air. Based on our examination of the interaction of an acoustic cavity with an external acoustic wave as discussed previously, it seems reasonable to hypothesize that the essential directionally sensitive response of the ears of these two flies might also be strongly influenced by the back cavity. It may be that by using an appropriate back cavity behind the tympana, details of the tympanal anatomy (or diaphragm design in microphones) may play a secondary rather than primary role in determining the response to sound.

While not addressed in this initial study, it is possible that the incorporation of the cavity with the sensing structures as employed here could have a number of additional practical benefits. We suspect that because the thickness of the viscous boundary layer grows as the frequency of the sound is reduced, low frequency, i.e., long wavelength pressure fluctuations will tend to be attenuated by the cavity.

40   J. Acoust. Soc. Am. **157** (1), January 2025

Lai *et al.*

This could be beneficial in attenuating long wavelength, non-acoustic fluctuations due to wind. Minimizing undesirable wind noise is always a challenge in directional microphones that are designed to detect pressure gradients. A flow-sensing microphone equipped with a properly designed cavity may prove very beneficial in attenuating this wind noise.

ACKNOWLEDGMENTS

AUTHOR DECLARATIONS
Conflict of Interest

The authors have no conflicts to disclose.

DATA AVAILABILITY

The data that support the findings of this study are available within the article.

Ando, S., Kurihara, T., Watanabe, K., Yamanishi, Y., and Ooasa, T. (**2009**). "Novel theoretical design and fabrication test of biomimicry directional microphone," in *Proceedings of Transducers 2009 International Solid-State Sensors, Actuators and Microsystems Conference*, June 21–25, Denver, CO, pp. 1932–1935.

Bartel, H. W., and McAvoy, J. M. (**1981**). *Cavity Oscillation in Cruise Missile Carrier Aircraft* (DTIC, Wright-Patterson Airforce Base, OH).

Bathellier, B., Steinmann, T., Barth, F. G., and Casas, J. (**2012**). "Air motion sensing hairs of arthropods detect high frequencies at near-maximal mechanical efficiency," J. R Soc. Interf. **9**, 1131–1143.

Bauer, R., Zhang, Y., Jackson, J. C., Whitmer, W. M., Brimijoin, W. O., Akeroyd, M., Uttamchandani, D., and Windmill, J. F. (**2016**). "Housing influence on multi-band directional mems microphones inspired by *Ormia ochracea*," in *Proceedings of 2016 IEEE Sensors*, October 30–November 3, Orlando, FL, pp. 1–3.

Bauer, R., Zhang, Y., Jackson, J. C., Whitmer, W. M., Brimijoin, W. O., Akeroyd, M. A., Uttamchandani, D., and Windmill, J. F. (**2017**). "Influence of microphone housing on the directional response of piezoelectric mems microphones inspired by *Ormia ochracea*," IEEE Sens. J. **17**(17), 5529–5536.

Cui, W., Bicen, B., Hall, N., Jones, S. A., Degertekin, F. L., and Miles, R. N. (**2006**). "Optical sensing inadirectional memsmicrophone inspired by the ears of the parasitoid fly, *Ormia ochracea*," in *Proceedings of the 19th IEEE International Conference on Micro Electro Mechanical Systems*, January 22–26, Istanbul, Turkey, pp. 614–617.

Dagamseh, A., Bruinink, C., Droogendijk, H., Wiegerink, R., Lammerink, T., and Krijnen, G. (**2010**). "Engineering of biomimetic hair-flow sensor arrays dedicated to high-resolution flow field measurements," in *Proceedings of the Sensors 2010*, November 1–4, Waikoloa, HI, pp. 2251–2254.

Droogendijk, H., Casas, J., Steinmann, T., and Krijnen, G. (**2014**). "Performance assessment of bio-inspired systems: Flow sensing mems hairs," Bioinspir. Biomim. **10**(1), 016001.

Fletcher, N. H., and Hill, K. (**1978**). "Acoustics of sound production and of hearing in the bladder cicada *Cystosoma Saundersii* (Westwood)," J. Exp. Biol. **72**(1), 43–55.

Göpfert, M. C., and Robert, D. (**2000**). "Nanometre–range acoustic sensitivity in male and female mosquitoes," Proc. R. Soc. Lond. B **267**(1442), 453–457.

Ishfaque, A., and Kim, B. (**2017**). "Fly *Ormia Ochracea* inspired mems directional microphone: A review," IEEE Sens. J. **18**(5), 1778–1789.

Knudsen, E. I. (**1980**). "Sound localization in birds," in *Comparative Studies of Hearing in Vertebrates* (Springer, New York), pp. 289–322.

Lai, J., Farahikia, M., Liu, Z., Yiang, Y., Ke, C., and Miles, R. (**2024**). "Effect of size on the thermal noise and acoustic response of viscous-driven microbeams," J. Acoust. Soc. Am. **155**(4), 2561–2576.

Lai, J., Karimi, M., and Miles, R. (**2022**). "Methods for accurate acoustic characterization with ultra-low noise and minimal effect from reflection wave," J. Acoust. Soc. Am. **152**(4), A194.

Larsen, O. N., Christensen-Dalsgaard, J., and Jensen, K. K. (**2016**). "Role of intracranial cavities in avian directional hearing," Biol. Cybernet. **110**, 319–331.

Liu, H., Yu, M., and Zhang, X. (**2008**). "Biomimetic optical directional microphone with structurally coupled diaphragms," Appl. Phys. Lett. **93**(24), 243902.

Mahesh, K., Ranjith, S. K., and Mini, R. (**2024**). "Recent advancements in Helmholtz resonator based low-frequency acoustic absorbers: A critical review," Arch. Comput. Methods Eng. **31**(4), 2079–2107.

Mason, M. J. (**2016**). "Internally coupled ears in living mammals," Biol. Cybernet. **110**, 345–358.

Michelsen, A., Popov, A., and Lewis, B. (**1994**). "Physics of directional hearing in the cricket *Gryllus bimaculatus*," J. Comp. Physiol. A **175**, 153–164.

Miles, R. (**2016**). "Acoustically coupled microphone arrays," J. Vib. Acoust. **138**(6), 064503.

Miles, R., and Hoy, R. (**2006**). "The development of a biologically-inspired directional microphone for hearing aids," Audiol. Neurotol. **11**(2), 86–94.

Miles, R., Robert, D., and Hoy, R. (**1995**). "Mechanically coupled ears for directional hearing in the parasitoid fly *Ormia ochracea*," J. Acoust. Soc. Am. **98**(6), 3059–3070.

Miles, R. N. (**2020**). *Physical Approach to Engineering Acoustics* (Springer, New York).

Miles, R. N., Su, Q., Cui, W., Shetye, M., Degertekin, F. L., Bicen, B., Garcia, C., Jones, S., and Hall, N. (**2009**). "A low-noise differential microphone inspired by the ears of the parasitoid fly *Ormia ochracea*," J. Acoust. Soc. Am. **125**(4, Part 1), 2013–2026.

Rahaman, A., and Kim, B. (**2019**). "Fly-inspired mems directional acoustic sensor for sound source direction," in *Proceedings of the 20th International Conference on Solid-State Sensors, Actuators and Microsystems & Eurosensors XXXIII (TRANSDUCERS & EUROSENSORS XXXIII)*, June 23–27, Berlin, Germany, pp. 905–908.

Rahaman, A., and Kim, B. (**2020a**). "A low-noise bio-inspired piezoelectric mems directional microphone for noise monitoring," in *Proceedings of INTER-NOISE and NOISE-CON Congress and Conference*, August 23–26, Seoul, Korea, pp. 5183–5187.

Rahaman, A., and Kim, B. (**2020b**). "Sound source localization by *Ormia ochracea* inspired low–noise piezoelectric mems directional microphone," Sci. Rep. **10**(1), 9545.

Robert, D. (**2005**). "Directional hearing in insects," in *Sound Source Localization* (Springer, New York), pp. 6–35.

Robert, D., Miles, R., and Hoy, R. (**1999**). "Tympanal hearing in the sarcophagid parasitoid fly *Emblemasoma* sp.: The biomechanics of directional hearing," J. Exp. Biol. **202**(14), 1865–1876.

Shah, M. A., Shah, I. A., Lee, D.-G., and Hur, S. (**2019**). "Design approaches of mems microphones for enhanced performance," J. Sens. **2019**(1), 294528.

Strutt, J. W. (**1916**). "The theory of the Helmholtz resonator," Proc. R. Soc. London, Ser. A **92**(638), 265–275.

Sung, P.-H., Chen, J.-Y., Yen, K-h., and Wu, C-y (**2007**). "CMOS compatible directional microphone," in *Proceedings of the 2007 International Microsystems, Packaging, Assembly and Circuits Technology*, October 1–3, Taipei, Taiwan, pp. 149–152.

Tao, J., and Yu, X. B. (**2012**). "Hair flow sensors: From bio-inspiration to bio-mimicking. a review," Smart Mater. Struct. **21**(11), 113001.

Vossen, C., Christensen-Dalsgaard, J., and Leo van Hemmen, J. (**2010**). "Analytical model of internally coupled ears," J. Acoust. Soc. Am. **128**(2), 909–918.

J. Acoust. Soc. Am. **157** (1), January 2025

Lai *et al.*   41

Zhang, Y., Bauer, R., Jackson, J. C., Whitmer, W. M., Windmill, J. F., and Uttamchandani, D. (**2018**). "A low-frequency dual-band operational microphone mimicking the hearing property of *Ormia ochracea*," J. Microelectromech. Syst. **27**(4), 667–676.

Zhang, Y., Bauer, R., Whitmer, W. M., Brimijoin, W. O., Uttamchandani, D., Windmill, J. F., and Jackson, J. C. (**2017**). "Development of a biologically inspired mems microphone," in *Proceedings of the 2017 IEEE Sensors Conference*, October 29–November 1, Glasgow, UK, pp. 1–3.

Zhang, Y., Windmill, J. F., and Uttamchandani, D. (**2014**). "Biomimetic mems directional microphone structures for multi-band operation," in *Proceedings of IEEE Sensors 2014*, November 2–5, Valencia, Spain, pp. 440–443.

Zhou, J., Lai, J., Menda, G., Stafstrom, J. A., Miles, C. I., Hoy, R. R., and Miles, R. N. (**2022**). "Outsourced hearing in an orb-weaving spider that uses its web as an auditory sensor," Proc. Natl. Acad. Sci. U.S.A. **119**(14), e2122789119.

Zhou, J., Li, B., Liu, J., Jones, W. E., Jr., and Miles, R. N. (**2018**). "Highly-damped nanofiber mesh for ultrasensitive broadband acoustic flow detection," J. Micromech. Microeng. **28**(9), 095003.

Zhou, J., and Miles, R. N. (**2017**). "Sensing fluctuating airflow with spider silk," Proc. Natl. Acad. Soc. U.S.A. **114**, 12120–12125.

42   J. Acoust. Soc. Am. **157** (1), January 2025

Lai *et al.*